Materials Transactions, Vol. 66, No. 1 (2025) pp. 44 to 49

Characterization of δNi_2Si Precipitates in Cu-Ni-Si Alloy by Small-Angle X-ray Scattering, Small-Angle Neutron Scattering, and Atom Probe Tomography*[1]

Hirokazu Sasaki[1,*2], Syunta Akiya[2], Kuniteru Mihara[3], Yojiro Oba[4], Masato Onuma[5], Jun Uzuhashi[6] and Tadakatsu Ohkubo[6]

[1]*Analysis Technology Center, Furukawa Electric Co., Ltd., Yokohama 220-0073, Japan*
[2]*Material Laboratory, Furukawa Electric Co., Ltd., Nikko 321-1493, Japan*
[3]*Electronics Component Material Division, Furukawa Electric Co., Ltd., Tokyo 100-8322, Japan*
[4]*Department of Mechanical Engineering, Toyohashi University of Technology, Toyohashi 441-8580, Japan*
[5]*Applied Quantum Science and Engineering, Faculty of Engineering, Hokkaido University, Sapporo 060-8628, Japan*
[6]*Research Center for Magnetic and Spintronic Materials, National Institute for Materials Science, Tsukuba 305-0047, Japan*

The strength of a Cu-Ni-Si alloy can be improved by finely dispersing Ni-Si-based compounds as precipitates into the Cu matrix through heat treatment. This requires quantitatively evaluating the size distribution and dispersion state to investigate the strengthening effect of the precipitate. In this work, we utilized transmission electron microscopy, small-angle X-ray scattering (SAXS), small-angle neutron scattering (SANS), and atom probe tomography (APT) to analyze these Ni-Si precipitates. The APT results showed two types of diffusion layers at the interface between the Cu matrix and precipitates. The alloy contrast variation method was used to examine the difference in SAXS and SANS intensity in absolute units, which indicated that the δNi_2Si precipitates are distorted. [doi:10.2320/matertrans.MT-D2024005]

(Received September 2, 2024; Accepted October 22, 2024; Published December 25, 2024)

Keywords: *transmission electron microscopy, small-angle x-ray scattering, small-angle neutron scattering, atom probe tomography, copper-nickel-silicon alloy, δNi_2Si precipitate*

1. Introduction

As electronic devices such as smartphones have become smaller, lighter, and more powerful, their electronic components have also become smaller and increased in performance. The requirements for copper alloy strips used in conductive parts such as leads and connectors of these electronic components are also increasing, requiring materials with both higher strength and conductivity than that of conventional materials. Cu-Ni-Si alloys have been known to exhibit high strength and conductivity after heat treatment, where Ni-Si compounds are dispersed finely within the copper matrix.

Transmission electron microscopy (TEM) is a key method for analyzing Ni-Si precipitates dispersed in the copper matrix, and makes it possible to evaluate the shape, size, density, and crystal structure of the precipitates [1–6]. This method is widely used for initial analysis.

In addition to TEM, the present study used atom probe tomography (APT) to analyze the size, shape, and composition of the precipitates. In the APT method, the 2D position-sensitive detector detects the ions that have evaporated from the surface of the needle-shaped sample's apex, and the obtained data are reconstructed as 3D atom maps at the nanometer scale. At the same time, the type of atoms can be identified by the time of flight in which the evaporated atoms reach the detector. The objective of APT investigation is to analyze the size, shape, and composition of precipitates on the order of several nanometers to tens of nanometers in Cu-Ni-Si alloys. The feature of APT that enables 3D visualization on the nanometer order can be effectively utilized to analyze structures with 3D geometries, in contrast to TEM, which is mainly a 2D analysis method.

Small-angle X-ray scattering (SAXS) is effective for quantitatively evaluating the number density, shape, etc. of precipitates in metals [7–12]. The measurement volume of SAXS is determined by the diameter of the irradiated X-ray beam and the thickness of the sample, and under typical metal measurement conditions, it is several million times larger than the observation volume of TEM, making it suitable for quantifying statistical values such as the average size of precipitates.

In this study, small-angle neutron scattering (SANS) was used in addition to SAXS to evaluate precipitates in Cu-Ni-Si alloys. SANS uses neutrons as the irradiation beam, which offers various advantages over SAXS. First, its strong material permeability makes it possible to measure thick samples. For copper measurements, neutrons can pass through a few millimeters of thickness, eliminating the need to polish the sample to the thickness required for SAXS measurements. As a result, the measurement volume to be 100,000 to 1,000,000 times larger than that of SAXS, which is important for gaining a more accurate understanding of the correlation between the electrical and mechanical properties of the metal products and precipitates. In addition, the scattering length of neutrons is not proportional to the atomic number, unlike that of X-rays, and neutron contrast also differs from that of X-rays. By using the contrast difference between neutrons and X-rays, information such as the composition and density of precipitates can be obtained [9–12]. Lastly, neutrons have spin, which enables analysis of magnetic materials. However, this feature is not generally used in the analysis of copper alloys.

*[1]This Paper was Originally Published in Japanese in J. Japan Inst. Copper **62** (2023) 85–89. The abstract and captions of Fig. 3 and 4 have been slightly modified.

*[2]Corresponding author, E-mail: hirokazu.sasaki@furukawaelectric.com

In this study, the structure of precipitates in copper alloys was analyzed in detail by utilizing these various analytical methods.

2. Experimental Procedure

2.1 Specimens

The specimens were Cu-Ni-Si Corson alloy containing 2.5 mass% Ni and 0.6 mass% Si. These were melted, cast, heat-treated, rolled, annealed, and solution heat-treated. Aging precipitation heat treatment was then conducted. SAXS and SANS measurements were conducted on the Cu-Ni-Si alloy samples at aging temperatures of 425, 450, 500, and 550°C, in addition to solution annealing only samples. The aging time was 2 h.

2.2 TEM observation

TEM samples were prepared using a focused ion beam (FIB) method. SIINT–3050TB was used for processing, and the Ga ion beam acceleration voltage was 30 kV. After FIB thin film processing, Ar ion milling at 2 kV was conducted. TEM observation was conducted using a JEOL JEM-2100 Plus, and a JEOL JEM-ARM200F was used for scanning TEM (STEM) observation. The electron beam acceleration voltage was 200 kV. High-angle annular dark field (HAADF) STEM images were taken in the STEM observations.

2.3 APT observation

Samples for APT measurements were prepared using an FIB. A Ga ion beam with an acceleration voltage of 30 kV was used to prepare a needle-shaped sample, and a 5-kV ion beam was used for final cleaning. A FEI Helios G4UX was used as the FIB. In this measurement, a LEAP5000XS was used, which has higher spatial resolution and detection efficiency than those used in previous studies [13, 14]. The measurement temperature was 30 K. An ultraviolet light with a wavelength of 355 nm was used as the pulsed laser to assist evaporation [15].

2.4 SAXS measurement

The samples were polished to a thickness of approximately 20 μm. A Rigaku NANO-Viewer was used as the laboratory system. A Mo–Kα X-ray source was used, and the energy of the incident X-ray was 17.47 keV. The sample-to-detector distance was 0.5 m. Ultra-SAXS (USAXS) measurements were also conducted at the beamline BL08B2 of SPring-8. The energy of the incident X-ray was 18 keV, and the sample-to-detector distance was 16 m. The laboratory SAXS profile was converted to the absolute value of the intensity using glassy carbon [16]. A single SAXS profile was created by connecting the USAXS profile in accordance with the intensity of the laboratory SAXS profile.

2.5 SANS measurement

The sample was approximately 2.1 mm thick. The measurements with camera lengths of 0.8 m and 9 m took 100 minutes and 40 minutes, respectively. The SANS profiles measured with the two camera lengths were combined to form a single SANS profile. The measurements were conducted at room temperature. The irradiated neutron beam was about 15 mm in diameter. SANS measurements were conducted using the SANS-J beamline installed in the JRR3 research reactor at the Japan Atomic Energy Agency. Absolute intensities were measured using Al standards for neutron irradiation. Compared with the measurements conducted in the previous studies [13, 14], this measurement differs in that the q-range is wider and absolute value processing was conducted. Therefore, the fitting process carried out and the profile intensity can be discussed.

3. Results and Discussions

3.1 TEM observation results

The bright-field TEM image is shown in Fig. 1. Numerous precipitates about 10 nm in size were observed in the left region of the TEM image. Contrast due to strain was observed in the copper matrix surrounding the precipitates. Furthermore, precipitates nearly 100 nm in size were also observed, as seen in the right area of the TEM image. Approximately one precipitate 50 nm to 100 nm in size was observed in every 1 μm square of the TEM field of view. This was also observed in the samples that had only been solution treated, indicating a phase that existed before the aging precipitation heat treatment. An enlarged HAADF-STEM image of one of the precipitates is shown in Fig. 2. Analysis of this image revealed that the precipitated phase was δNi_2Si, as previously reported [13, 14].

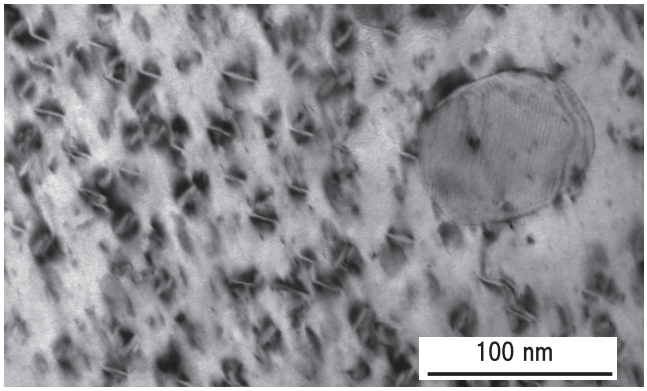

Fig. 1 Bright-field TEM image of 550°C heat-treated copper alloy.

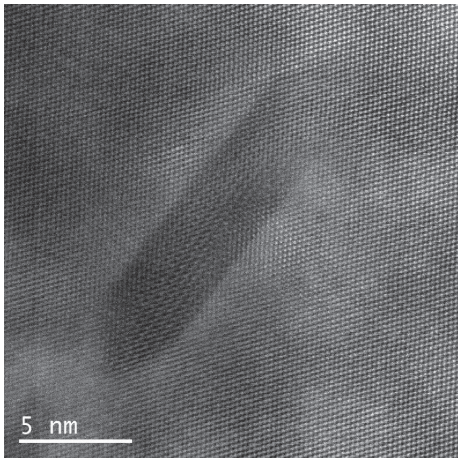

Fig. 2 HAADF-STEM image of δNi_2Si precipitate.

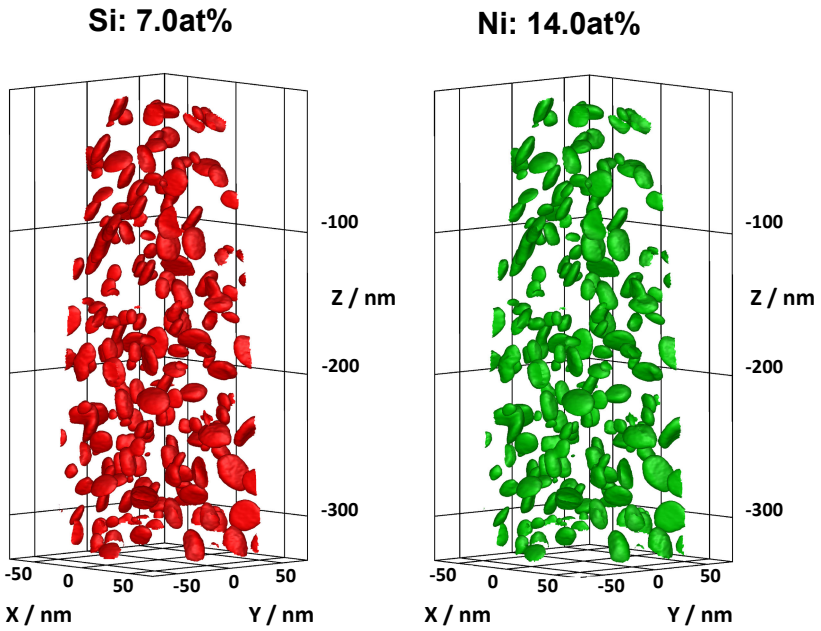

Fig. 3 3D atom map obtained by APT (iso-concentration-surfaces of Ni at 14 at% and Si at 7 at%). (online color)

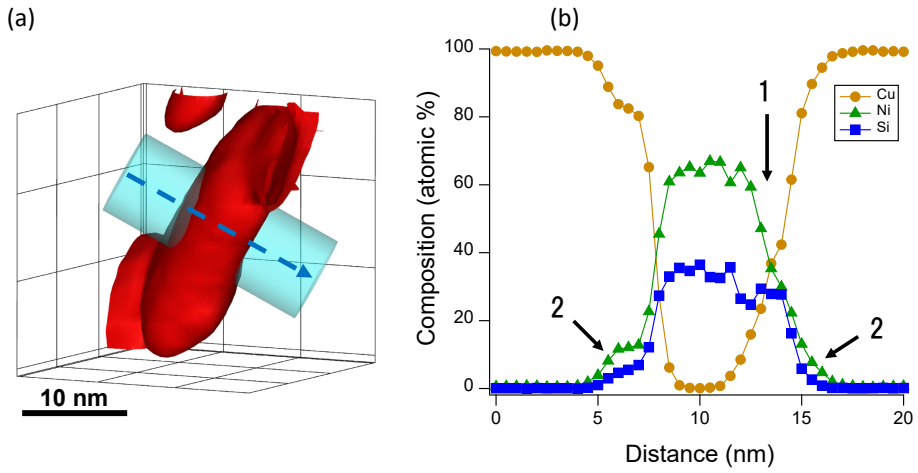

Fig. 4 Si 3D atom map of single precipitate (iso-concentration-surfaces of Si at 7 at%) and composition profiles obtained by APT. (online color)

3.2 APT observation results

Figure 3 shows the analysis results of a sample heat-treated at 550°C using an APT. The use of ultraviolet laser pulses made it possible to stably acquire data from a wide area, as shown in Fig. 3 [17]. In this figure, the iso-concentration surface of 14 atomic% Ni and 7 atomic% Si are shown. Within this field of view, the distributions of Ni and Si are almost the same, and the precipitated phase is not spherical but ellipsoidal, close to a disk.

To analyze the compositional details within the precipitates, the APT result of one of the precipitates is shown in Fig. 4. Figure 4(a) shows the iso-concentration surface of 7 atomic% Si. Figure 4(b) shows the composition profile within the precipitate created in the direction indicated by the arrow in the figure. As shown in the figure, the precipitating phase is Ni_2Si since the ratio of Ni to Si is 2:1 in the center. Interdiffusion of Ni, Si, and Cu at the interface between the precipitated phase and the Cu matrix was also observed. A closer look at the diffusion area reveals two characteristics as indicated by arrows 1 and 2. In the region indicated by arrow 1, the Si composition is constant and the Ni composition decreases toward the Cu matrix. This region is considered to be $\delta(Ni_{1-y}, Cu_y)_2Si$ as suggested by Yi *et al.* [18]. In the region indicated by arrow 2, Ni and Si diffuse into the copper matrix at less than 10%. Figure 5 shows a model diagram of the precipitated phase estimated from these APT results.

3.3 SAXS and SANS measurement results

The measurement results of SAXS and SANS are shown in Figs. 6 and 7. Each figure shows the small-angle scattering profiles of the solution-treated and heat-treated samples at aging temperatures of 425, 450, 500, and 550°C, respectively. Compared with the solution-treated Corson alloy, the 425°C aging sample shows a shoulder indicating the formation of nanoparticles in the region of $q = 0.4$ to $2\,nm^{-1}$. As the aging heat treatment temperature increases, the shoulder indicating scattering moves toward the low-q

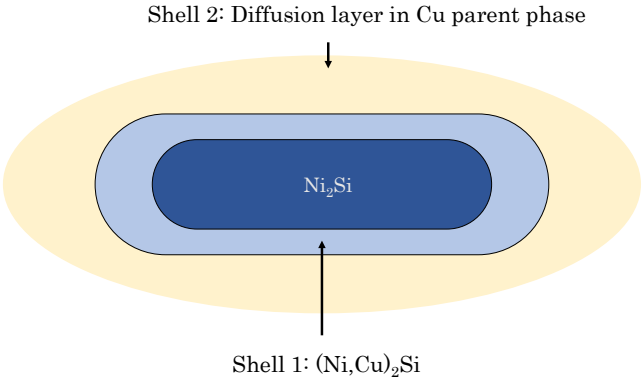

Fig. 5 Core-shell model of precipitate in copper alloy. (online color)

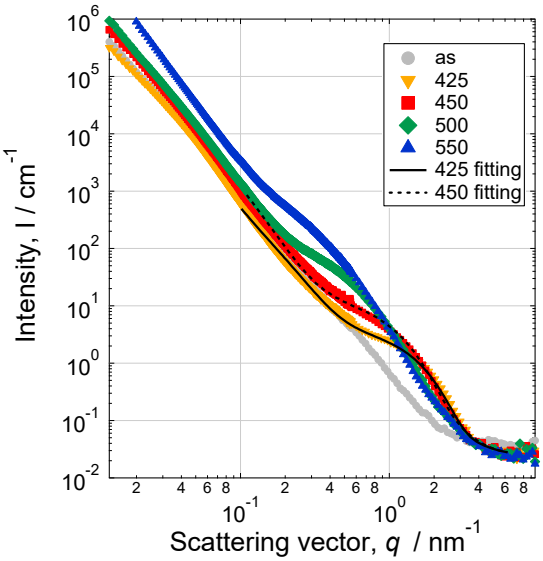

Fig. 6 SAXS profiles of copper alloys. (online color)

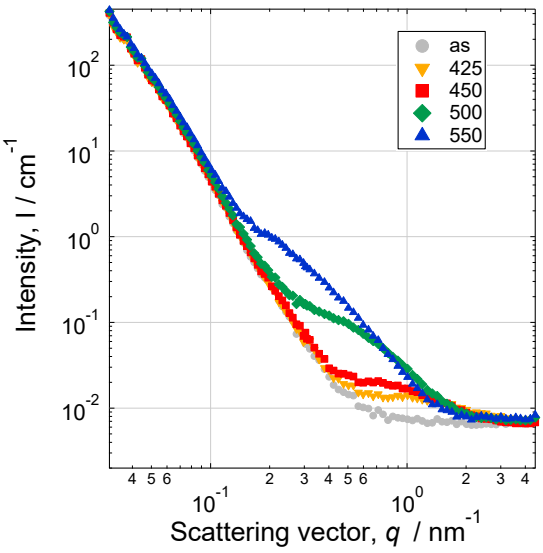

Fig. 7 SANS profiles of copper alloys. (online color)

side. These results indicate that the Ni-Si precipitates gradually become coarser.

The Ni-Si precipitates in the 425 and 450°C aging samples could be fitted as spherical particles, with an average particle

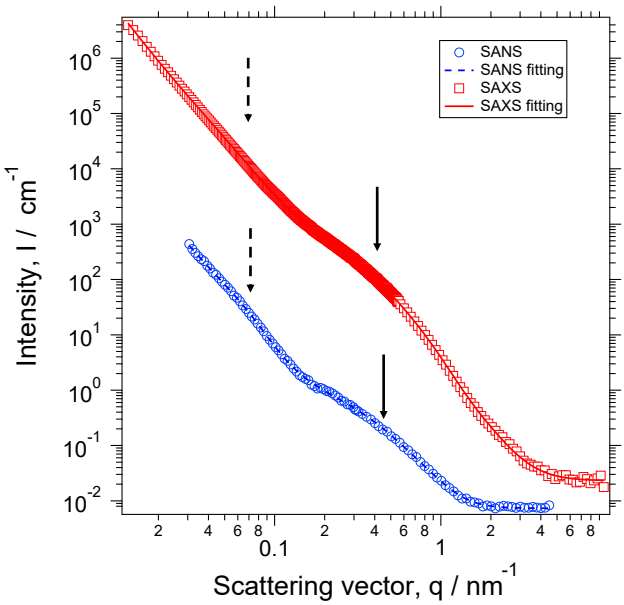

Fig. 8 SAXS and SANS profiles of 550°C heat-treated copper alloys. (online color)

size of 2.2 nm for the 425°C aging sample and 2.6 nm for the 450°C aging sample. The precipitates of the 500 and 550°C aging samples are disk-like ellipsoids, as shown by the results of the APT, so it is appropriate to fit them with this shape.

3.4 SAXS and SANS profiles analysis

The SAXS and SANS profiles were analyzed on the basis of the APT results of the precipitates. Although the precipitates of the 500 and 550°C aging samples differ in size, their profile shapes are similar, so the analysis was conducted on the 550°C aging sample. From the results of the APT, the precipitates of the 550°C aging sample are assumed to be disk-like ellipsoids. Therefore, SAXS and SANS profiles were fitted on the basis of this assumption. In this case, the axis ratio of the ellipsoid was assumed to be 0.3. Phases larger than 50 nm observed in the TEM image in Fig. 1 are assumed to be spherical for fitting. In this fitting, the background caused by incoherent scattering, which generally appears in the high-q region above $q = 2\,\mathrm{nm}^{-1}$, is set as a constant value, and the background resulting from the coarse structure, which is more prominent in the low-q region, is taken as q^{-4}.

The fitting results are shown by the solid line in Fig. 8. The shoulder near $q = 0.3\,\mathrm{nm}^{-1}$, indicated by the arrow in the figure, corresponds to the precipitates. The shoulder around $q = 0.05\,\mathrm{nm}^{-1}$, indicated by the dashed arrow, corresponds to coarse phases. Assuming a spherical model and fitting using a SANS profile, the average radius was 38 nm.

The precipitates were fitted with SAXS profiles, and the average major axis radius of the ellipsoid was 8.9 nm. Conversely, the ellipsoid fitted with SANS profiles had an average major axis radius of 6.6 nm. The difference in the results between SAXS and SANS is due to the difference in the scattering contrast of the $\delta(Ni_{1-y}, Cu_y)_2Si$ diffusion layer, where Cu diffuses into the precipitated phase. As mentioned in previous studies [13, 14], the scattering contrast of the

$\delta(Ni_{1-y}, Cu_y)_2Si$ diffusion layer in the copper matrix is large for X-rays and small for neutrons. Therefore, the precipitates were measured to be larger in SAXS and smaller in SANS.

Subsequently, analyses were conducted using the alloy contrast variation method, which estimates the composition and density of the precipitates from the intensity ratio of the absolute SAXS and SANS profiles [9–12]. The scattering lengths corresponding to the elements differ between X-rays and neutrons, and this difference is reflected in the intensity ratios of SAXS and SANS profiles. The scattering length density difference $\Delta\rho$ for the δNi_2Si precipitates in the copper matrix is different between X-rays and neutrons. This difference is between the scattering length density of the matrix phase and that of the precipitated phase [9]. If the difference in scattering length density of X-rays is $\Delta\rho_x$ and that of neutrons is $\Delta\rho_n$, the intensity ratio of SAXS and SANS is $\Delta\rho_x^2/\Delta\rho_n^2$ when the precipitate is a single phase. When the precipitate phase in the copper matrix is δNi_2Si, $\Delta\rho_x^2/\Delta\rho_n^2$ is theoretically 80. In this calculation, the lattice constants of δNi_2Si are assumed to be $a = 0.706$ nm, $b = 0.499$ nm, and $c = 0.372$ nm [19], and the density is 7.37 g/cm3. Conversely, the intensity ratio calculated from the SAXS and SANS profiles of the 550°C aging sample was 345. One reason for this difference is the effect of the diffusion layer observed in the APT analysis. Since the composition in this region is different from that of δNi_2Si, the scattering length-density difference is also different [13, 14]. In addition, it was previous reported that the δNi_2Si precipitate phase and the copper matrix phase are lattice-matched, i.e., the lattice parameter of the δNi_2Si precipitate phase is larger and its density is smaller due to lattice misfit [18], which can cause the difference in the intensity ratio. If the density of δNi_2Si is 7.01 g/cm3, $\Delta\rho_x^2/\Delta\rho_n^2$ is 345, which can be interpreted as the intensity ratio of the SAXS and SANS profiles. If we assume that the lattice constant of the precipitate phase is uniformly large, this corresponds to a 1.8% increase in the lattice constant, but in reality, the lattice constant is not uniform within the precipitate phase, and the strain of each crystal axis is also considered to be non-uniform. From the aforementioned experimental results, the intensity ratio of the SAXS and SANS profiles should be interpreted taking into account the effects of both the lattice strain and diffusion layer. However, detailed modeling is a subject for future work.

4. Conclusion

(1) The APT results suggest the existence of two types of diffusion layers at the interface between the precipitate phase and copper matrix.
(2) In the SAXS and SANS profiles, the precipitates of the 550°C aging specimen can be fitted as ellipsoids. The major axis radius of the precipitates was 8.9 nm in SAXS and 6.6 nm in SANS, which may be due to the difference in X-ray and neutron contrast of the diffusion layer.
(3) The intensity ratios of absolute SAXS and SANS profiles were analyzed using the alloy contrast variation method, the findings of which suggest that the precipitate phase is not a simple δNi_2Si. This may be due to the density change of the δNi_2Si phase caused by the lattice strain between the precipitated phase and the copper matrix and the diffusion layer observed in the APT, which may affect the intensity of the SAXS and SANS profiles. Detailed modeling will be conducted in the future, taking these findings into account.

Acknowledgments

The STEM observations were supported by the Microstructure Analysis Platform of the University of Tokyo, which is part of the Nanotechnology Platform funded by the Ministry of Education, Culture, Sports, Science and Technology of Japan. Laboratory SAXS measurements were conducted in collaboration with the Institute for Integrated Radiation and Nuclear Science, Kyoto University. SPring-8 SAXS measurements were conducted at the Hyogo Prefecture Beamline BL08B2 (Proposal No. 2019A3337). SANS measurements were conducted at the SANS-J of JRR3 in JAEA (Proposal No. 2021A-A43). APT measurements of copper alloys were conducted with the cooperation of Kyoko Suzuki of the National Institute for Materials Science.

REFERENCES

[1] S.A. Lockyer and F.W. Noble: Precipitate structure in a Cu-Ni-Si alloy, J. Mater. Sci. **29** (1994) 218–226.
[2] H. Fujiwara, T. Sato and A. Kamio: Effect of Alloy Composition on Precipitation Behavior in Cu-Ni-Si Alloys, J. Japan Inst. Metals **62** (1998) 301–309 (in Japanese).
[3] A. Araki, I. Kobayashi, T. Sato, K. Hirose and T. Eguchi: Copper and Copper Alloys **52** (2013) 14–18 (in Japanese).
[4] Q. Lei, Z. Li, C. Dai, J. Wang, X. Chen, J.M. Xie, W.W. Yang and D.L. Chen: Effect of aluminum on microstructure and property of Cu–Ni–Si alloys, Mater. Sci. Eng. A **572** (2013) 65–74.
[5] Y. Jia, M. Wang, C. Chen, Q. Dong, S. Wang and Z. Li: Orientation and diffraction patterns of δ-Ni2Si precipitates in Cu–Ni–Si alloy, J. Alloy. Compd. **557** (2013) 147–151.
[6] A. Araki, W.J. Poole, E. Kobayashi and T. Sato: Twinning Induced Plasticity and Work Hardening Behavior of Aged Cu–Ni–Si Alloy, Mater. Trans. **55** (2014) 501–505.
[7] K. Miyazawa, Y. Tanaka and T. Fujii: Size and Morphology Analysis of Precipitates Dispersed in Cu Alloys by Small Angle X–ray Scattering, Copper and Copper Alloys **58** (2019) 103–108 (in Japanese).
[8] Y. Ohba: Ferrum **18** (2013) 257–259 (in Japanese).
[9] M. Onuma: Analysis of Microstructure by Small-Angle X-ray Scattering, Materia **54** (2015) 616–620 (in Japanese).
[10] M. Onuma: Characterization of Nano-size Heterogeneities by Small-angle-scattering, Surf. Sci. **33** (2012) 278–283 (in Japanese).
[11] M. Ohnuma, J. Suzuki, S. Ohtsuka, S.W. Kim, T. Kaito, M. Inoue and H. Kitazawa: A new method for the quantitative analysis of the scale and composition of nanosized oxide in 9Cr-ODS steel, Acta Mater. **57** (2009) 5571–5581.
[12] Y. Oba, S. Koppoju, M. Ohnuma, T. Murakami, H. Hatano, K. Sasakawa, A. Kitahara and J. Suzuki: Quantitative Analysis of Precipitate in Vanadium-microalloyed Medium Carbon Steels Using Small-angle X-ray and Neutron Scattering Methods, ISIJ Int. **51** (2011) 1852–1858.
[13] H. Sasaki, S. Akiya, Y. Oba, M. Ohnuma, A.D. Giddings and T. Okubo: Characterization of Precipitated Phase in Cu–Ni–Si Alloy by Small Angle X–ray Scattering, Small Angle Neutron Scattering and Atom Probe Tomography, Copper and Copper Alloys **60** (2021) 309–314 (in Japanese).
[14] H. Sasaki, S. Akiya, Y. Oba, M. Onuma, A.D. Giddings and T. Ohkubo: Characterization of Precipitated Phase in Cu–Ni–Si Alloy by Small-Angle X-ray Scattering, Small Angle Neutron Scattering and

Atom Probe Tomography, Mater. Trans. **63** (2022) 1384–1389.
[15] T. Okubo, Y. Chen, M. Kozuka and K. Takarano: Nanoscale Characterization of Ceramics by Laser Assisted Atom Probe Tomography, Materia **50** (2011) 397–403 (in Japanese).
[16] F. Zhang, J. Ilavsky, G.G. Long, J.P.G. Quintana, A.J. Allen and P.R. Jemian: Glassy Carbon as an Absolute Intensity Calibration Standard for Small-Angle Scattering, Metall. Mater. Trans. A **41** (2010) 1151–1158.
[17] J. Uzuhashi, T. Ohkubo and K. Hono: Development of automated tip preparation for atom probe tomography by using script-controlled FIB-SEM, Ultramicroscopy **247** (2023) 113704.
[18] J. Yi, Y. Jia, Y. Zhao, Z. Xiao, K. He, Q. Wang, M. Wang and Z. Li: Precipitation behavior of Cu-3.0Ni-0.72Si alloy, Acta Mater. **166** (2019) 261–270.
[19] K. Toman: The structure of Ni_2Si, Acta Crystallogr. **5** (1952) 329–331.